

pubs.acs.org/JPCC Article

Healing Se Vacancies in Bi₂Se₃ by Ambient Gases

Sharmila N. Shirodkar,* Gregory M. Stephen,* Aubrey T. Hanbicki,* Adam L. Friedman,* and Pratibha Dev*



Cite This: J. Phys. Chem. C 2022, 126, 16877-16884



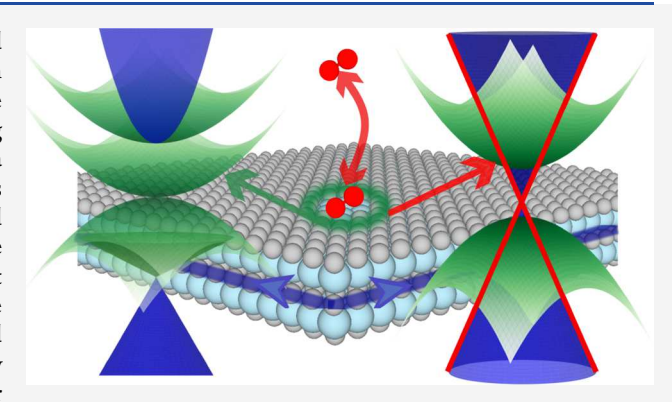
ACCESS

Metrics & More

Article Recommendations

Supporting Information

ABSTRACT: Selenium (Se) vacancies are the most abundant and unavoidable n-type defects in the topological insulator, bismuth selenide (Bi₂Se₃). A recent study has shown that the surface Se vacancies not only *n*-dope the system but also result in the splitting of the Dirac cone associated with the surface and the emergence of a nonlinear state pinned at the Fermi level due to the interactions between surface-, defect-, and quantum-well states. In this combined theoretical and experimental work, we show how the defective surfaces of Bi₂Se₃ slabs can be healed by adsorption of different gases. Depending on the adsorbates, we find that the band structure of Bi₂Se₃ either reverts back to its pristine form or exhibits localized adsorbate bands near the Fermi level. Notably, our density functional theory calculations show that both atomic and molecular



oxygen are isoelectronic to Se, binding strongly to the vacancy position. Along with counterdoping (p-doping) of Bi_2Se_3 (as reported by earlier studies), oxygen adsorption completely restores the Dirac structure of the surface states. Our experiments confirm that annealing intrinsically n-doped Bi_2Se_3 samples with oxygen reduces the carrier density by $\approx 6\%$. This is a reversible process, with the Bi_2Se_3 slab reverting back to the original carrier concentration on vacuum annealing, thus confirming the healing of vacancies by oxygen. We distinguish the possible features of the adsorbates that can be used to a priori predict their effects on the electronic structure of the Bi_2Se_3 slab after adsorption. Our results provide a foundation for a general strategy for the in situ engineering of the band structure of the Bi_2Se_3 family of topological insulators by quenching Se vacancies.

INTRODUCTION

Three-dimensional (3D) topological insulators are an exotic class of materials that exhibit an insulating bulk and topologically nontrivial surface states ^{1,2} that are protected against time reversal invariant perturbations such as crystal defects, distortions, and nonmagnetic impurities. ³⁻⁶ The surface states disperse linearly and intersect one another forming a Dirac cone, with a Dirac point at the Fermi level. The robustness of these states against perturbations, coupled with spin-momentum locking that prohibits backscattering processes, makes topological insulators advantageous for application in spintronics and quantum computing. The position of the Fermi level depends on the quality of the sample, its aging effects, and the ambient conditions. The ability to control and manipulate the position of the Fermi level with respect to the Dirac cone will strongly influence the performance of these devices.

Bi₂Se₃ is a strong 3D topological insulator with a large bulk band gap of 0.3 eV.^{7,8} It has been widely studied because its surface states fall in the bulk gap and are isolated from the bulk states. The surface states in Bi₂Se₃ samples undergo changes with time, which is also known as aging.^{9–12} This manifests as an increase in the binding energy of the topologically protected surface states, that is, the shift of the surface states and Dirac point deeper into the valence band, indicating an effective *n*-

doping of the surface. Possible explanations for the aging effect include the following: change in the van der Waals (vdW) distance between the layers, 13 adsorption of molecules/atoms at the surface, 9,14 and/or formation of Se vacancies. $^{15-17}$ As the Se vacancies are the most abundant intrinsic defects in $\rm Bi_2Se_3$, and those on the surface are exposed to the environment and are reactive, it is important to understand how different gases, whether present intentionally or unintentionally, modify the defect structure and affect the surface states. In addition, understanding the interaction of vacancies with gases could potentially alter the aging process by either stopping or slowing down the degradation.

Previous works have shown that O_2 doping of $Bi_2Se_3^{18-20}$ reduces the n-doping of the samples by binding strongly to Se vacancies. On the other hand, N_2 dissociates at the surface vacancies and binds to them, shifting the Dirac point toward the Fermi level, that is, p-doping the sample. However, previous

Received: July 21, 2022
Revised: September 7, 2022
Published: September 21, 2022





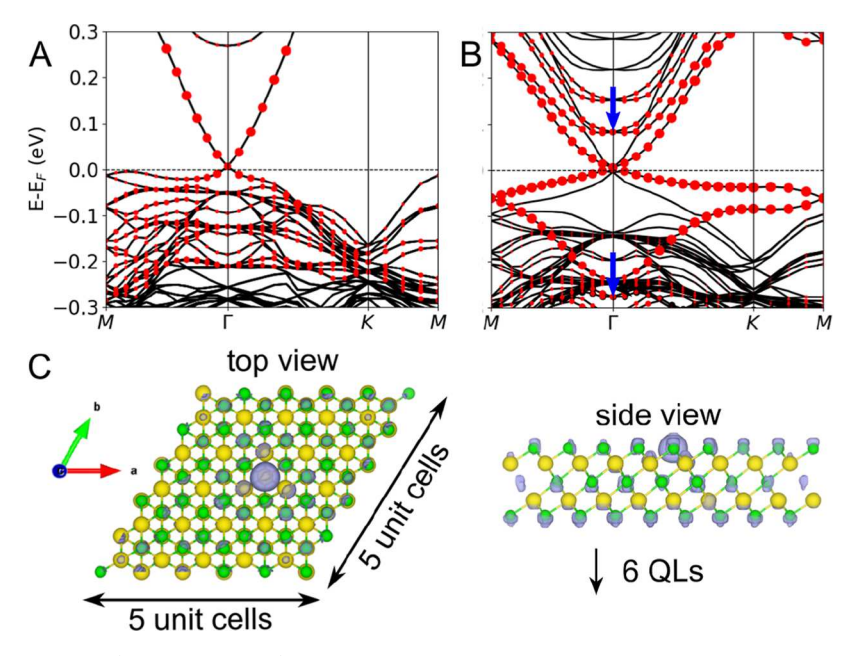


Figure 1. Electronic structure of Bi_2Se_3 ($5 \times 5 \times 7$ QL slab) with and without the Se vacancy and structural model of the vacancy site. Band structure of the (A) pristine and (B) defective Bi_2Se_3 slab with single Se vacancy at the surface. Reproduced from Shirodkar; Dev, "Nonlinear hybrid surface-defect states in defective Bi_2Se_3 ", The Journal of Physical Chemistry C 2022, 126, 11833–11839. Copyright 2022 American Chemical Society. The blue arrows indicate the surface states shifted into the conduction and valence bands due to hybridization with the defect. Red circles denote the contribution from the top QL. The surface states from the bottom layer are degenerate with the top layer surface states in the pristine case. (C) Top and side views of the top QL with a Se vacancy. Also shown is the isosurface of the charge density difference (between defective and pristine supercells), showing the pooling of electrons at the vacancy site. Bi (Se) atoms are shown as yellow (green) spheres and the charge density is shown in purple.

theoretical works^{20,21} studied these effects under very high doping/vacancy concentrations (in-plane 1014 cm-2 due to remarkably high cost of computations) that were much larger than those found in real experimental samples, thus limiting the applicability of the calculations. Furthermore, until recently, the subtle effects that result in the shifting and splitting of the Dirac cone associated with the defective surface layer were not understood.²² Shirodkar and Dev showed that the splitting of the Dirac cone associated with the defective surface is due to the interactions between the defect-, surface-, and quantum-well (QW)¹⁰ states. The adsorption of ambient gases at the defect site is expected to modify these interactions. Here, we explore in detail the effect of ambient gases (O, O2, N, N2, F, and F2) on both, the lattice and electronic structure of vacancies on the surface of Bi₂Se₃ for very low defect concentrations (in-plane 10¹³ cm⁻², i.e., 1.3%, as observed in real samples), using both experiments and first-principles calculations. To understand the correlation between the change in the electronic structure of Bi₂Se₃ and the adsorbed gas, we also analyze the physical attributes of the gases: a step toward possibly defining a descriptor that can predict the doping levels in the slab due to adsorbates.

METHODS

Computational Details. We used the SIESTA package ^{23,24} to carry out density functional theory (DFT) calculations. A plane wave mesh cutoff of 150 Ry was used for nonspinpolarized calculations and calculations including spinorbit interactions. The electron—ion interactions were modeled with fully relativistic norm-conserving pseudopotentials obtained from PseudoDojo, ^{25,26} with exchange correlation energy between electrons approximated by the GGA functional parameterized by Perdew–Burke–Ernzerhof. ²⁷ A double-zeta polarized basis set was used in our calculations.

In order to minimize the interaction between the top and bottom layers in Bi₂Se₃, we used seven quintuple layers (QLs), in which each QL consisted of Se-Bi-Se-Bi-Se layers. This ensures a Dirac cone at the Fermi level with the band gap <1 meV. In addition, to ensure that our calculations have experimentally relevant defect densities, we used a 5 × 5 inplane supercell. A single Se vacancy was created on the top surface in the $5 \times 5 \times 7$ QL Bi₂Se₃ supercell, and the adsorbate was added at the defective site. Using the reasonable assumption that the defect site-adsorbate chemistry is unaffected by the lower vdW bonded layers, we carried out the calculations in two steps: (a) first, we relaxed the composite structure consisting of an adsorbate on a single 5 × 5 defective QL, yielding the adsorption energy and (b) we then translated this defective QL with the adsorbate onto a 5×5 supercell slab of six QLs, yielding a 5 \times 5 \times 7 QL stack. This composite structure with the adsorbate on a $5 \times 5 \times 7$ QLs was used to calculate the band structure, capturing the effect of the adsorbate on the surface and vacancy states. This two-step process made these very expensive calculations more tractable.

In the first step, the structural relaxation calculations of the $5 \times 5 \times 1$ QL slabs with adsorbates were carried out without spin—orbit coupling effects, and the structure was relaxed until the Hellman—Feynman forces on the atoms were <0.04 eV/Å. We relaxed the structures under both, without and with vdW interactions (i.e., by adding a dispersion potential of the Grimme type²⁸). We found that the inclusion of vdW interactions compressed the QL layer by $\approx 1.8\%$ and lowered the adsorption energies by $\approx 0.2-0.3$ eV with respect to the layer without vdW interactions. Hence, we report the adsorption energies with vdW interactions (in agreement with²¹); however, we use the structures without vdW interactions to calculate the electronic band structure in the $5 \times 5 \times 7$ QL slab. The Brillouin Zone

(BZ) integrations were carried out over a $3 \times 3 \times 1$ Monkhorst Pack k-point mesh for a $5 \times 5 \times 1$ QL slab.

Next, we translated the defect + adsorbate layer (only the top Bi and Se layer, relaxed without vdW interactions) onto six pristine QLs, keeping the interlayer separation fixed to that of bulk to determine the electronic structure. This $5 \times 5 \times 7$ QL supercell slab consisted of 875 atoms. The BZ integrations for the $5 \times 5 \times 7$ QL slab were carried only at the BZ center, that is, Γ -point. A vacuum of 24 Å was included in the nonperiodic direction to minimize the interaction between the periodic images of the defects and adsorbates for both the $5 \times 5 \times 1$ and $5 \times 5 \times 7$ QL slabs.

Experimental Details. In order to confirm our theoretical predictions, a Hall bar of Bi₂Se₃, previously characterized in depth, ²⁹ was annealed under O₂, vacuum, and N₂ gas to observe the change in carrier density, and thereby the Fermi level, with gas adsorption. Experiments were performed in a cryogen-free magneto-cryo-probe station capable of reaching temperatures between 10 K and 500 K. Gas inlets were used to expose the sample space to gas without exposing it to the atmosphere. We first measured the baseline sample carrier density at 10 K. Next, we annealed the sample in situ at 450 K for 1 h under vacuum or 0.5 bar N_2 gas. Then, we measured the carrier density again at 10 K. The sample was then annealed again in situ at 450 K for 1 h under 0.5 bar O₂ gas before the carrier density was again measured at 10 K. Finally, we annealed the sample at 450 K for 1 h under either vacuum or 0.5 bar N₂ gas and measured the carrier density again at 10 K. The sample was kept in a N2 dry box between the N₂ and vacuum cycles. Measured values were compared between different sets of contacts on the same Hall bar to estimate the uncertainty.

RESULTS AND DISCUSSION

Figure 1A is the plot of band structure for a pristine $5 \times 5 \times 7$ QL Bi₂Se₃ slab showing the Dirac cone structure of the topologically protected states at the Fermi level. On the other hand, the presence of the Se vacancy in the surface layer not only *n*-dopes the system but also leads to a number of subtle effects (discussed in detail by Shirodkar and Dev²²) that went unreported in the earlier works. 30,31 For example, it splits the Dirac cone such that the bottom part of the Dirac cone moves to \approx -225 meV below the Fermi level and the top part hybridizes with the conduction band (details elsewhere,²² see Figure 1B, blue arrows). The hybridization of the Dirac cone with the defect states not only shifts the Dirac cone into the valence and conduction bands but also introduces nonlinearity in them and pins the Fermi level to the parabolic defect bands. 22 These nonlinear defect states were mistakenly identified as the defective layer's Dirac cone in a previous work³⁰ since they too prohibit spin-backscattering processes at the Fermi level and also connect the valence and conduction bands through topologically protected defective surface states, just like the surface states in pristine Bi₂Se₃ slabs. Because the nonlinearity of these states implies an increase in effective mass of electrons and hence a decrease in their mobility, it is crucial to understand the physics behind the evolution of the electronic structure of the defective Bi₂Se₃ slab with adsorbed gases to predict their applicability and performance in devices. Furthermore, due to symmetry breaking and the doping of the defective QL (see Figure 1C), a number of QW states emerge inside the bulk gap in the conduction band due to band bending at the vacuum and the defective top QL (see Figure 1B, energy range of 0.1-0.3 eV). 10

Adsorption Energies: Adsorbates on the $5 \times 5 \times 1$ QL

Slab. In order to determine which of the common gases/molecules both p-dope and restore the band structure of the defective Bi_2Se_3 , we investigated the adsorption of O, O_2 , N, N_2 , F, and F_2 at the vacancy site (see the Supporting Information for results on H_2O and P). For the diatomic molecules O_2 , N_2 , and F_2 , we consider both parallel and perpendicular orientations of the molecule with respect to the surface of the slab (see Figure

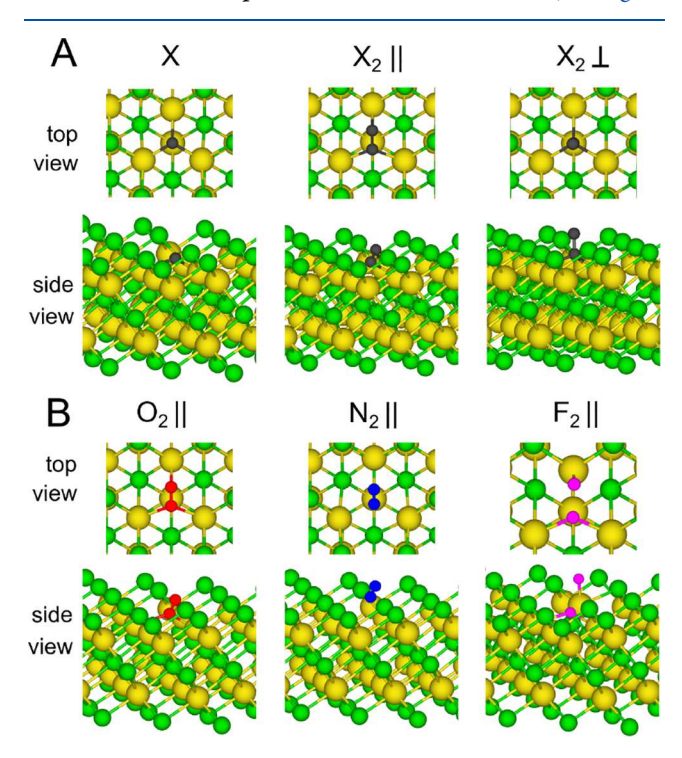


Figure 2. Structural orientation of the adsorbate at the vacancy site for a single atom (X) and a diatomic molecule (X_2) . (A) The diatomic molecule can be oriented with its axis parallel ($\|$) or perpendicular (\bot) to the slab, and we consider both the orientations. Bi (Se) atoms are shown as yellow (green) spheres, and the adsorbate is shown in black. (B) Relaxed structures of O_2 (red), N_2 (orange), and F_2 (pink) molecules at the Se vacancy. Note that the $\|$ and \bot orientations for both O_2 and F_2 relax to the same structure shown here.

2A). The adsorption energy ($E_{\rm adsorption}$) with respect to the molecule for a 5 × 5 × 1 QL slab is calculated as follows

$$E_{\text{adsorption}} = E_{\text{vacancy}+\text{adsorbate}} - E_{\text{vacancy}} - E_{\text{adsorbate}}/n$$
 (1

where E_{vacancy} is the energy of the 5 × 5 × 1 QL slab with Se vacancy, $E_{\text{vacancy+adsorbate}}$ is the energy of the slab with the adsorbate at the vacancy site, and $E_{\text{adsorbate}}$ is the energy of the molecule. n=1 if the adsorbate is in the molecular form or n=2 if it is in the atomic form.

The calculated adsorption energies are given in Table 1. Clearly, oxygen and fluorine bind strongly to the vacancy site, whereas nitrogen only physisorbs 21 and most likely desorbs from the surface at finite temperatures. We find that the O_2 molecule relaxes parallel to the slab, irrespective of the original \parallel or \perp orientation. However, the fluorine molecule in both parallel and perpendicular orientation dissociates and the atoms attach to two different Bi atoms adjacent to the vacancy. This explains the similar adsorption energies for the two structures (\parallel and \perp), and henceforth, we will discuss results for only one of the dissociated structures. N_2 binds weakly to the surface, in agreement with a

Table 1. Adsorption Energy (in eV) of O, N, and F at the Vacancy Site with Respect to Their Molecular Forms^a

adsorbate	О	N	F
X	-3.02	1.47	-3.82
$X_2 \parallel$	-3.29	0.32	-6.42
X, ⊥	-1.61	0.08	-6.66

"X and X_2 signify atomic and molecular forms of the adsorbate, respectively; \parallel and \perp correspond to the parallel and perpendicular orientations of the molecule, respectively. Note that the vdW interactions are included in the adsorption energies.

previous report. Of Settschalk et al. predicted that a N_2 molecule can dissociate near a pair of Se vacancies and then strongly bind to the surface. This p-dopes the sample exposed to N_2 and consequently the shifts of the Dirac point closer to the Fermi level. However, we find that such a situation is less probable since (a) formation of a vacancy pair at the surface is less likely and depends on the sample quality and (b) atomic nitrogen is magnetic (discussed in detail later) and opens a gap in the surface states. Hence, we suspect that the p-doping that they report in their work is a result of other contaminants or has a different origin and needs further exploration. Therefore, we will only focus on the parallel configuration in the following discussion. The final relaxed structures of the molecules at the

vacancy are shown in Figure 2B; the quantitative details of the structure are discussed in a later section.

Electronic Structure: Adsorbates on the $5 \times 5 \times 7$ QL Slab. The band structures of oxygen, nitrogen, and fluorine (in both atomic and parallel molecular forms) are given in Figure 3, where the contribution from the adsorbent (in the top QL) is highlighted in blue (red). The adsorbate states hybridize strongly with the top QL states and contribute to all the states near the Fermi level. In addition, O, O2, 20 and F2 heal the vacancy and restore the top QL Dirac cone to the Fermi level (see Figure 3A,C). The wave functions at the Dirac point plotted in Figure 3B,D, also confirm the preservation of the top QL surface state. It is important to note that among the three adsorbates, atomic oxygen brings the electronic structure of the defective Bi₂Se₃ slab closest to that of a pristine slab (compared with Figure 1B). Even if O₂ and F₂ manage to counter dope and compensate fully for the *n*-doping of the top QL, states at the Mpoint (near the Fermi level) shift deeper into the valence band and the band structure does not exactly resemble that of a pristine slab. We also find that although a single F atom at the vacancy acts as a p-dopant, it cannot compensate (accept) for all the electrons in the absence of Se. This can be understood on the basis of formal oxidation states of the ions involved, which is -1for fluorine as opposed to -2 for oxygen, with the latter having

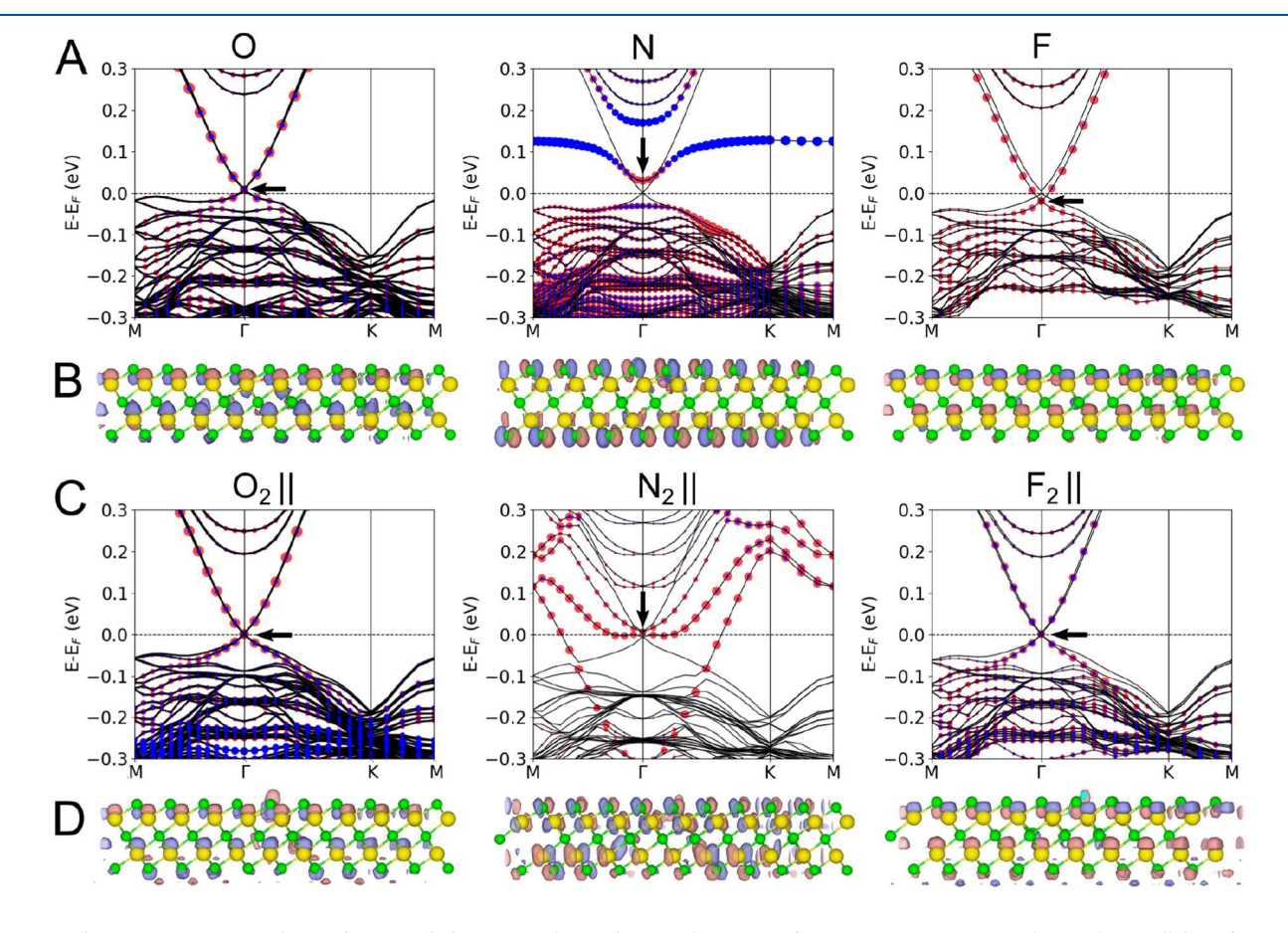


Figure 3. Electronic structure and wave functions belonging to the top layer at the Γ -point for $X=O,N,F,O_2,N_2$, and F_2 in the parallel configuration. Band structure of (A) O (left column), N (middle column), and F (right column) and (C) O_2 || (left column), N_2 || (middle column), and F_2 || (right column). Red (blue) circles denote the contribution from the top QL and the adsorbate. The charge density isosurface of the wave function (denoted by a black arrow in the band structure) at the Γ-point is shown in (B) for X=O,N, and F and (D) for $X=O_2,N_2$, and F_2 (i.e., below their respective band structures). Bi (Se) atoms are shown as yellow (green) spheres. The opposite phases of the wave functions are denoted by red and blue colors in the charge density plots. Note that we only show the top QL of the seven QLs in the $S\times S\times 7$ QL slab for ease of visualization, and these structures were relaxed without vdW interactions.

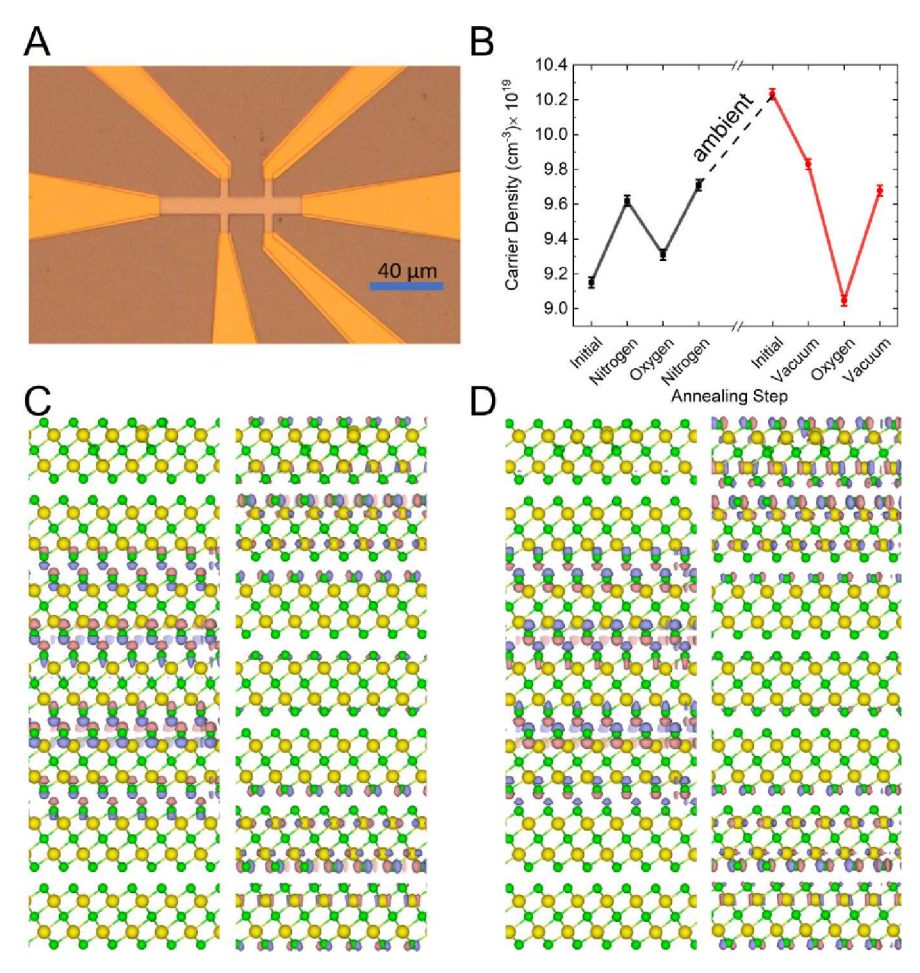


Figure 4. Experimental results and QW states. (A) Optical image of a Bi_2Se_3 Hall bar used in this study. Electrical contacts are electron beam-deposited Ti/Au, described elsewhere. (B) Plot of variation in carrier density with control annealing in N_2 (black) and vacuum (red). The Γ-point charge density isosurface of wave functions of (C) the LUMO of pristine Bi_2Se_3 at 0.27 eV and (D) QW state at 0.24 eV of O adsorbed at the Se vacancy on the surface. Note that the asymmetry in the structure due to O adsorption also introduces asymmetry in the QW states as compared to pristine Bi_2Se_3 . Bi (Se) atoms are shown as yellow (green) spheres. The opposite phases of the wave functions are denoted by red and blue colors in the charge density plots.

the same oxidation number (-2) as Se in Bi₂Se₃. Hence, the top QL still remains slightly *n*-doped (see Figure 3A,B, right column).

The N_2 configuration has the most unique band structure, which resembles that of a Se vacancy situated in the middle of the layer. 22 This is because N₂ does not bind to the vacancy (see Table 1) and only modifies the dispersion of the bands by changing the environment of the vacancy. On comparing the band structure with that of a Se vacancy sandwiched between two Bi layers (refer to ref 22) in the top QL, we find similarities in the dispersion of the defect/nonlinear bands at the Fermi level. We postulate that the N₂ molecule acts similar to Bi layers, that is, it screens the vacancy from vacuum that modifies the defect, hence mimicking the electronic band structure of the vacancy deeper in the layer. The contribution of the N₂ molecule to the bands at the Fermi level is also negligible in comparison with the other adsorbates. The charge density plot of the wave function at the Fermi level (see Figure 3B, middle column) shows that the contribution is mostly from the surface state and the N₂ contribution is negligible. Quite interestingly, atomic nitrogen is magnetic with a moment of $\approx 0.5 \mu_{\rm B}$, which destroys the topological protection of the top surface state and opens up a gap of ≈0.06 eV. Our calculations for phosphorus (isoelectronic to N) doping of the Se vacancy show that the adsorbate still

remains magnetic but without any significant opening of the gap (see the Supporting Information for details). However, it does not energetically bind to the vacancy ($E_{\text{adsorption}} = 0.28 \text{ eV}$ with vdW corrections). This implies that although elements belonging to group 15 of the periodic table can be used to manipulate the Dirac cone back to the Fermi level, they will do so under special conditions (e.g., pressure, strain, and doping) since they do not adsorb under equilibrium (as captured by ab initio calculations). We note that none of the other molecular/ atomic configurations support a magnetic moment, thus ensuring topological protection to the surface states, as seen from our band structure and wave function plots. For completeness, we also calculate the electronic structure for H₂O adsorbed at the Se vacancy and find that its influence on the band structure is similar to that of N₂ (see the Supporting Information for details).

To confirm that the adsorption of O_2 at the Se vacancy site heals the defect, whereas N_2 does not attach to the defective site, we carried out annealing experiments (results are shown in Figure 4). As discussed in the Methods section, transport measurements are made on a sample patterned into a standard Hall bar, as shown in Figure 4A. In particular, the carrier concentration is recorded after the sample is exposed to various gases while being annealed to 450 K, as shown in Figure 4B. We

find a clear decrease in the carrier density between both control anneals (vacuum and N₂) and the O₂ anneal. Upon O₂ annealing, the sample shows an 8% and 2% reduction in carrier density relative to vacuum annealing and N2 annealing, respectively. These decreases are well above measurement uncertainties and are significant. Note that there is a modest increase in carrier concentration after exposure to the ambient conditions in the laboratory and is likely a byproduct of the O₂ treatment. As oxygen heals defects, it not only fills vacancies but also likely replaces other more weakly bound chemisorbed species. Nitrogen annealing will drive off some of the oxygen, but exposure to atmosphere can lead to other chemisorbed species such as CO₂ and H₂O, displacing even more oxygen. The vacuum anneal then drives off the newly adsorbed species, restoring the carrier concentration. Since *n*-doping of the sample is a result of Se vacancies, $^{15-17,32}$ annealing in O_2 heals these Se vacancies on the surface. Therefore, we observe a decrease in the carrier density, confirming that O2 leads to antiaging effects in the sample. 9,11 We also find that the carrier density is similar for both of the control annealing steps (in vacuum and N₂), further supporting the theoretical conclusion from our DFT results that N₂ does not bind to the vacancies/impurities.

In addition to confirming the seamless passivation of Se vacancies by oxygen molecules, that is, the return of the Dirac cone back to the Fermi level, we focus our attention on the QW states in the conduction band. We note that these states persist for all of the adsorbate elements/gases and lie at ≈ 0.24 eV for O, 0.19 eV for O₂, 0.25 eV for N, 0.19 eV for N₂, 0.20 eV for F, and 0.18 eV for F₂. They are lower in energy than the bulk conduction band minimum, which is at 0.27 eV for the pristine case (see Figure 1A) and higher than the QW + defect + Dirac cone hybrid state at \approx 0.1 eV (see Figure 1B). On closer inspection of the wave functions of these doubly degenerate QW states at the Γ -point (see Figure 4D and the Supporting Information for details), we find that they are made up of one state localized to the bulk and the other to the outer QLs and are almost similar to the lowest unoccupied molecular orbital (LUMO) states of the pristine Bi₂Se₃ slab (see Figure 4C) with slight asymmetry due to the adsorbed molecule/atom. Hence, we note that even if O, O₂, and F₂ electronically replace Se, the breaking of structural inversion symmetry due to the adatom/ molecule itself shifts the QW states inside the bulk gap and is related to how strongly the symmetry is broken. Since F₂ breaks apart, the structure is more asymmetric and the shift is larger, that is, QW state appears at \approx 0.18 eV, in comparison with O, which breaks the symmetry weakly and its QW state emerges at \approx 0.24 eV. We note that the N₂ molecule is an exception to this observation since it does not bond to the vacancy, and its QWstate wave functions are closer to those in the vacancy case (see Figure 1B and the Supporting Information for details). Previous works^{20,21} missed this nuance since they focused mainly on the restoration of the Dirac cone to the Fermi level, but our detailed study clearly highlights these differences and also explains their origin.

Given that materials such as Bi₂Se₃ will likely be used under ambient conditions, it is instructive to determine the physicochemical properties of different possible adsorbates that have the biggest impact on those of Bi₂Se₃. Hence, in order to gain a greater insight into the characteristics of the adsorbates and their effect on the band structure of defective Bi₂Se₃, we plot the most important features, (a) difference in valence electrons with respect to Se, (b) Bi-adsorbate distance, and (c) the average number of electrons gained by the adsorbate (same as

electronegativity) (see Figure 5), and relate them to the shift in the Dirac cone with respect to the Fermi level due to the

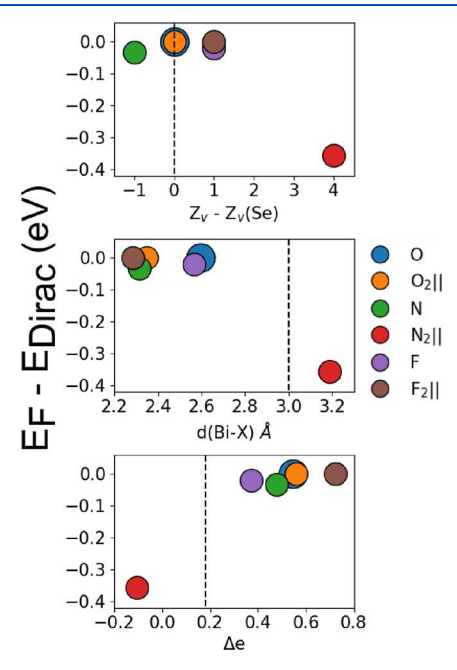


Figure 5. Shift in Dirac cone relative to Fermi energy as a function of different physicochemical properties/attributes of the adsorbates: (A) difference in valence electrons with respect to Se $[Z_{\nu}-Z_{\nu}(Se)]$, (B) Biadsorbate distance $[d(Bi-X) \mbox{ Å}]$, and (C) average number of electrons gained by the adsorbate (Δe) . The dashed black lines indicate the values for Se in a pristine slab.

adsorbate. First, we consider the relationship between the shift in the Dirac cone and the difference between valence electrons with respect to Se (see Figure 5, top panel). Both O and O_2 lie on the vertical, dashed black line, which indicates that they both have the same electronic configuration as Se.²⁰ It is not surprising that upon adsorption of O and O2, the band structure reverts back to that for a pristine Bi₂Se₃ slab. However, it is clear that a consideration of mere valency does not explain why F₂ behaves the same as oxygen, even when it has an additional electron/atom as compared to Se in its outer shell. Similarly, the average atom/molecule and Bi distance is not related with the changes in the band structure (see Figure 5, middle panel). The adsorbate-Bi distance for N₂, which does not heal the vacancy, is much closer to the Bi-Se bond length, as compared to other adsorbates. The most important attribute that affects the band structure is the amount of charge gained by the adsorbate (electronegativity) (see Figure 5, bottom panel). The plot shows that if the electron gain is >0.5e per adsorbate atom/molecule $(O, O_2, F, and F_2)$, the *n*-doping is fully compensated for and the Dirac cone shifts back to the Fermi level. Since atomic F only gains 0.37 e, the Dirac cone shifts to ≈ -20 meV below the Fermi level. However, since N is magnetic, it opens up a gap in the surface states of the top QL and does not bring the Dirac cone near the Fermi level. Finally, N₂, which does not bind to the vacancy, shows no electron gain. We find that F2 gains the maximum charge, 0.73e > O, $O_2(0.55e) > N(0.47e) > F(0.37e)$ $> N_2 (-0.1e).$

CONCLUSIONS

We confirm that the intrinsic (n-) doping level in defective Bi_2Se_3 slabs can be engineered with the adsorption of ambient

gases. Unlike other gases that only dope the defective layer, we show that atomic nitrogen opens up a gap in the surface states of the defective layer on account of it being magnetic, in contrast to an earlier work that did not consider magnetization of the adsorbate. Interestingly, we also find that the nonmagnetic adsorbates such as N_2 and H_2O , which are weakly and/or nonbonding, change the dispersion of the surface states at the Fermi level. In particular, the band structure of the adsorbate-slab composite for N_2 or H_2O resembles the electronic structure of Se vacancies situated in a different Wyckoff positions in the same layer. 22

We conclude that electronegativity/electron gain of the adsorbate is the most important attribute determining the shift of the Dirac cone relative to the Fermi level and therefore the doping level in the defective Bi₂Se₃ slab. Our results show that elements with larger electronegativity than Se (except nitrogen) counteract the effects of the Se vacancies in this material and shift the Dirac cone back to the Fermi level. Hence, one can also counter the effects of aging by deliberately exposing the sample to oxygen. We note that none of the elements/gases show the ability to shift the Dirac point above the Fermi level, that is, hole dope the ideal Bi₂Se₃ slab. Finding such a *p*-dopant/ adsorbate remains a topic of future research.

ASSOCIATED CONTENT

Supporting Information

The Supporting Information is available free of charge at https://pubs.acs.org/doi/10.1021/acs.jpcc.2c05175.

Results for water and phosphorus adsorption at vacancy sites and charge densities of the QW states (PDF)

AUTHOR INFORMATION

Corresponding Authors

Sharmila N. Shirodkar — Department of Physics and Astronomy, Howard University, Washington, District of Columbia 20059, United States; occid.org/0000-0002-9040-5858; Email: sharmila.shirodkar@howard.edu

Gregory M. Stephen — Laboratory for Physical Sciences, College Park, Maryland 20740, United States; ⊚ orcid.org/0000-0002-8477-4438; Email: gstephen@lps.umd.edu

Aubrey T. Hanbicki — Laboratory for Physical Sciences, College Park, Maryland 20740, United States; Orcid.org/0000-0001-8200-0378; Email: hanbicki@lps.umd.edu

Adam L. Friedman — Laboratory for Physical Sciences, College Park, Maryland 20740, United States; Email: afriedman@ lps.umd.edu

Pratibha Dev — Department of Physics and Astronomy, Howard University, Washington, District of Columbia 20059, United States; Email: pratibha.dev@howard.edu

Complete contact information is available at: https://pubs.acs.org/10.1021/acs.jpcc.2c05175

Notes

The authors declare no competing financial interest.

ACKNOWLEDGMENTS

This work was supported by the W. M. Keck Foundation and the NSF grant no. DMR-1752840. We acknowledge the computational support provided by the Extreme Science and Engineering Discovery Environment (XSEDE) under Project PHY180014, which was supported by the National Science Foundation grant

no. ACI-1548562, and the Maryland Advanced Research Computing Center.

REFERENCES

- (1) Kane, C. L.; Mele, E. J. Quantum Spin Hall Effect in Graphene. *Phys. Rev. Lett.* **2005**, *95*, 226801.
- (2) Bernevig, B. A.; Hughes, T. L.; Zhang, S.-C. Quantum Spin Hall Effect and Topological Phase Transition in HgTe Quantum Wells. *Science* **2006**, *314*, 1757–1761.
- (3) Xu, Y.; Chiu, J.; Miao, L.; He, H.; Alpichshev, Z.; Kapitulnik, A.; Biswas, R. R.; Wray, L. A. Disorder enabled band structure engineering of a topological insulator surface. *Nat. Commun.* **2017**, *8*, 14081.
- (4) Miao, L.; Xu, Y.; Zhang, W.; Older, D.; Breitweiser, S. A.; Kotta, E.; He, H.; Suzuki, T.; Denlinger, J. D.; Biswas, R. R.; et al. Observation of a topological insulator Dirac cone reshaped by non-magnetic impurity resonance. *npj Quantum Mater.* **2018**, *3*, 29.
- (5) Zhong, M.; Li, S.; Duan, H.-J.; Hu, L.-B.; Yang, M.; Wang, R.-Q. Effect of impurity resonant states on optical and thermoelectric properties on the surface of a topological insulator. *Sci. Rep.* **2017**, *7*, 3971.
- (6) Teague, M.; Chu, H.; Xiu, F.-X.; He, L.; Wang, K.-L.; Yeh, N.-C. Observation of Fermi-energy dependent unitary impurity resonances in a strong topological insulator Bi2Se3 with scanning tunneling spectroscopy. *Solid State Commun.* **2012**, *152*, 747–751.
- (7) Zhang, H.; Liu, C.-X.; Qi, X.-L.; Dai, X.; Fang, Z.; Zhang, S.-C. Topological insulators in Bi2Se3, Bi2Te3 and Sb2Te3 with a single Dirac cone on the surface. *Nat. Phys.* **2009**, *5*, 438–442.
- (8) Xia, Y.; Qian, D.; Hsieh, D.; Wray, L.; Pal, A.; Lin, H.; Bansil, A.; Grauer, D.; Hor, Y. S.; Cava, R. J.; et al. Observation of a large-gap topological-insulator class with a single Dirac cone on the surface. *Nat. Phys.* **2009**, *5*, 398–402.
- (9) King, P. D. C.; Hatch, R. C.; Bianchi, M.; Ovsyannikov, R.; Lupulescu, C.; Landolt, G.; Slomski, B.; Dil, J. H.; Guan, D.; Mi, J. L.; et al. Large Tunable Rashba Spin Splitting of a Two-Dimensional Electron Gas in Bi,Se₃. *Phys. Rev. Lett.* **2011**, *107*, 096802.
- (10) Park, K.; Beule, C. D.; Partoens, B. The ageing effect in topological insulators: evolution of the surface electronic structure of Bi2Se3upon K adsorption. *New J. Phys.* **2013**, *15*, 113031.
- (11) Bianchi, M.; Guan, D.; Bao, S.; Mi, J.; Iversen, B. B.; King, P. D.; Hofmann, P. Coexistence of the topological state and a two-dimensional electron gas on the surface of Bi2Se3. *Nat. Commun.* **2010**, *1*, 128.
- (12) Hsieh, D.; Xia, Y.; Qian, D.; Wray, L.; Dil, J. H.; Meier, F.; Osterwalder, J.; Patthey, L.; Checkelsky, J. G.; Ong, N. P.; et al. A tunable topological insulator in the spin helical Dirac transport regime. *Nature* **2009**, *460*, 1101–1105.
- (13) Menshchikova, T. V.; Eremeev, S. V.; Chulkov, E. V. On the origin of two-dimensional electron gas states at the surface of topological insulators. *JETP Lett.* **2011**, 94, 106.
- (14) Bianchi, M.; Hatch, R. C.; Li, Z.; Hofmann, P.; Song, F.; Mi, J.; Iversen, B. B.; El-Fattah, Z. M. A.; Löptien, P.; Zhou, L.; et al. Robust Surface Doping of Bi2Se3 by Rubidium Intercalation. *ACS Nano* **2012**, *6*, 7009–7015.
- (15) Navrátil, J.; Horák, J.; Plecháček, T.; Kamba, S.; Lošťák, P.; Dyck, J.; Chen, W.; Uher, C. Conduction band splitting and transport properties of Bi2Se3. *J. Solid State Chem.* **2004**, *177*, 1704–1712.
- (16) Jafarpisheh, S.; Ju, A.; Janßen, K.; Taniguchi, T.; Watanabe, K.; Stampfer, C.; Beschoten, B. Reducing the Impact of Bulk Doping on Transport Properties of Bi-Based 3D Topological Insulators. *Phys. Status Solidi B* **2021**, 258, 2000021.
- (17) West, D.; Sun, Y. Y.; Wang, H.; Bang, J.; Zhang, S. B. Native defects in second-generation topological insulators: Effect of spin-orbit interaction on Bi₂Se₃. *Phys. Rev. B: Condens. Matter Mater. Phys.* **2012**, *86*, 121201.
- (18) Chen, Y. L.; Chu, J.-H.; Analytis, J. G.; Liu, Z. K.; Igarashi, K.; Kuo, H.-H.; Qi, X. L.; Mo, S. K.; Moore, R. G.; Lu, D. H.; et al. Massive Dirac Fermion on the Surface of a Magnetically Doped Topological Insulator. *Science* **2010**, *329*, 659–662.

- (19) Hsieh, D.; McIver, J. W.; Torchinsky, D. H.; Gardner, D. R.; Lee, Y. S.; Gedik, N. Nonlinear Optical Probe of Tunable Surface Electrons on a Topological Insulator. *Phys. Rev. Lett.* **2011**, *106*, 057401.
- (20) Koleini, M.; Frauenheim, T.; Yan, B. Gas Doping on the Topological Insulator Bi₂Se₃ Surface. *Phys. Rev. Lett.* **2013**, *110*, 016403.
- (21) Gottschalk, M.; Lee, M.-S.; Goodwin, E.; Mikolas, C.; Chasapis, T.; Chung, D. Y.; Kanatzidis, M.; Mahanti, S. D.; Tessmer, S. Evidence for nitrogen gas surface doping of the Bi2Se3 topological insulator. **2020**, arXiv preprint arXiv:2004.01631.
- (22) Shirodkar, S. N.; Dev, P. Nonlinear Hybrid Surface-Defect States in Defective Bi2Se3. *J. Phys. Chem. C* **2022**, *126*, 11833–11839.
- (23) Soler, J. M.; Artacho, E.; Gale, J. D.; García, A.; Junquera, J.; Ordejón, P.; Sánchez-Portal, D. The SIESTA method forab initioorder-Nmaterials simulation. *J. Phys.: Condens. Matter* **2002**, *14*, 2745–2779.
- (24) Cuadrado, R.; Cerdá, J. I. Fully relativistic pseudopotential formalism under an atomic orbital basis: spin—orbit splittings and magnetic anisotropies. *J. Phys.: Condens. Matter* **2012**, *24*, 086005.
- (25) van Setten, M.; Giantomassi, M.; Bousquet, E.; Verstraete, M.; Hamann, D.; Gonze, X.; Rignanese, G.-M. The PseudoDojo: Training and grading a 85 element optimized norm-conserving pseudopotential table. *Comput. Phys. Commun.* **2018**, 226, 39–54.
- (26) García, A.; Verstraete, M. J.; Pouillon, Y.; Junquera, J. The psml format and library for norm-conserving pseudopotential data curation and interoperability. *Comput. Phys. Commun.* **2018**, 227, 51–71.
- (27) Perdew, J. P.; Burke, K.; Ernzerhof, M. Generalized gradient approximation made simple. *Phys. Rev. Lett.* **1996**, 77, 3865.
- (28) Grimme, S. Semiempirical GGA-type density functional constructed with a long-range dispersion correction. *J. Comput. Chem.* **2006**, 27, 1787–1799.
- (29) Stephen, G. M.; Vail, O. A.; Lu, J.; Beck, W. A.; Taylor, P. J.; Friedman, A. L. Weak Antilocalization and Anisotropic Magnetoresistance as a Probe of Surface States in Topological Bi2TexSe3x Thin Films. *Sci. Rep.* **2020**, *10*, 4845.
- (30) Yan, B.; Zhang, D.; Felser, C. Topological surface states of Bi2Se3 coexisting with Se vacancies. *Phys. Status Solidi RRL* **2013**, *7*, 148–150.
- (31) Wang, S.; Zhang, P. Native point defects in Bi2Se3: A first-principles study. *Phys. Lett. A* 2020, 384, 126281.
- (32) Stephen, G. M.; Naumov, I.; Tyagi, S.; Vail, O. A.; DeMell, J. E.; Dreyer, M.; Butera, R. E.; Hanbicki, A. T.; Taylor, P. J.; Mayergoyz, I.; et al. Effect of Sn Doping on Surface States of Bi2Se3 Thin Films. *J. Phys. Chem. C* 2020, 124, 27082–27088.

□ Recommended by ACS

$\label{eq:conductivity} Ultrafast\ Anisotropic\ Evolution\ of\ Photoconductivity\ in\ Sb_2Se_3\ Single\ Crystals$

Huijie Liu, Ye Yang, et al.

JUNE 01, 2022

THE JOURNAL OF PHYSICAL CHEMISTRY LETTERS

RFAD 🗹

Percolation Process-Mediated Rich Defects in Hole-Doped PbSe with Enhanced Thermoelectric Performance

Jinchang Sun, Gangjian Tan, et al.

JULY 08, 2022

CHEMISTRY OF MATERIALS

READ 🗹

Competing Superior Electronic Structure and Complex Defect Chemistry in Quasi-One-Dimensional Antimony Chalcogenide Photovoltaic Absorbers

Baiyu Zhang and Xiaofeng Qian

JANUARY 05, 2022

ACS APPLIED ENERGY MATERIALS

RFAD **[**✓

Tailoring the Crystallographic Orientation of a ${\rm Sb}_2{\rm S}_3$ Thin Film for Efficient Photoelectrochemical Water Reduction

Minji Yang, Yanbo Li, et al.

JUNE 23, 2022

ACS CATALYSIS

READ 🗹

Get More Suggestions >